Published in final edited form as:

Eur J Nucl Med Mol Imaging. 2022 February ; 49(3): 861–870. doi:10.1007/s00259-021-05563-1.

ImmunoPET of trophoblast cell-surface antigen 2 (Trop-2) expression in pancreatic cancer

Weiyu Chen[#1,2,3], **Miao Li**[#2,4], **Muhsin H. Younis**[2], **Todd E. Barnhart**[2], **Dawei Jiang**[2], **Tuanwei Sun**[2], **Joshua M. Lang**[5,6], **Jonathan W. Engle**[2], **Min Zhou**[1,7], **Weibo Cai**[2,5]

[1]The Fourth Affiliated Hospital, Zhejiang University School of Medicine, Yiwu 322000, Zhejiang, China

[2]Departments of Radiology and Medical Physics, University of Wisconsin-Madison, Madison, WI 53792, USA

[3]International Institutes of Medicine, the Fourth Affiliated Hospital of Zhejiang University School of Medicine, Yiwu, Zhejiang, China

[4]Department of Cancer Precision Medicine, Med-X Institute, the First Affiliated Hospital of Xi'an Jiaotong University, Xi'an 710061, Shaanxi, China

[5]University of Wisconsin Carbone Cancer Center, Madison, WI 53705, USA

[6]Department of Medicine, University of Wisconsin-Madison, Madison, WI 53705, USA

[7]Institute of Translational Medicine, Zhejiang University, Hangzhou 310009, China

[#] These authors contributed equally to this work.

Abstract

Purpose—Without a standard test for pancreatic carcinomas, this highly lethal disease is normally diagnosed at its advanced stage, leading to a low survival rate of patients. Trophoblast cell-surface antigen 2 (Trop-2), a transmembrane glycoprotein, is associated with cell proliferation and highly expressed in most of solid epithelial tumors, including pancreatic cancer. A non-invasive method of imaging Trop-2 would greatly benefit clinical diagnosis and monitoring of pancreatic cancer. In the current study, ^{89}Zr-labeled anti-Trop-2 antibody (AF650) was recruited for the systemic evaluation of Trop-2 as an immunoPET target for pancreatic cancer imaging.

Methods—AF650 was conjugated with desferrioxamine (DFO) and then radiolabeled with ^{89}Zr. Trop-2 expression levels were determined in three pancreatic cancer cell lines (BxPC-3,

Min Zhou, zhoum@zju.edu.cn, Weibo Cai, wcai@uwhealth.org.
Weiyu Chen and Miao Li contributed equally to this work.

Supplementary Information The online version contains supplementary material available at https://doi.org/10.1007/s00259-021-05563-1.

Declarations

Research involving human participants and/or animals The current study does not include any studies associated with human participants. And this work follows all applicable guidelines (international, national, and/or institutional) for the care and use of animals.

Conflict of interest Weibo Cai is a scientific advisor, stockholder, and grantee of Focus-X Therapeutics, Inc. All other authors declare that they have no conflict of interest.

MIA PaCa-2, and AsPC-1) via western blot, flow cytometry, saturation binding assay, and immunofluorescence staining. The targeting capacity of ^{89}Zr-DFO-AF650 was evaluated in mouse models with subcutaneous xenograft of pancreatic cancers via PET imaging and bio-distribution studies. In addition, a Trop-2-positive orthotopic cancer model was recruited for further validating the targeting specificity of ^{89}Zr-DFO-AF650.

Results—BxPC-3 cells expressed high levels of Trop-2, while AsPC-1 and MIA PaCa-2 cells expressed low levels of Trop-2. Additionally, ^{89}Zr-DFO-AF650 exhibited high specificity to Trop-2 in BxPC-3 cells (K_d = 22.34 ± 2.509 nM). In subcutaneous xenograft models, about 28.8 ± 7.63%ID/g tracer accumulated in the BxPC-3 tumors at 120 h post injection, which was much higher than those reaching MIA PaCa-2 (6.76 ± 2.08%ID/g) and AsPC-1 (3.51 ± 0.69%ID/g) tumors (n = 4). More importantly, ^{89}Zr-DFO-AF650 could efficiently distinguish primary tumors in the orthotopic BxPC-3 cancer model, showing high correlation between PET imaging and bio-distribution and sensitivity.

Conclusions—^{89}Zr-DFO-AF650 can be effectively used to detect pancreatic cancer via Trop-2-mediated immunoPET in vivo, clearly revealing the great potential of Trop-2-based non-invasive imaging in pancreatic cancer detection and treatment monitoring.

Keywords

Positron emission tomography (PET); Trophoblast cell-surface antigen 2 (Trop-2); Pancreatic cancer; Monoclonal antibody (mAb); Molecular imaging; Zr-89

Introduction

The mortality rate of cancer is gradually decreasing, with a 29% overall decline of death in 2017 compared with that of 1991 [1]. Interestingly, the largest single-year drop (2.2%) has been observed in 2014. Despite this, the incidence of pancreatic cancer is increasing. Pancreatic carcinoma, the most dangerous type of pancreatic cancer, shows a 5-year survival rate of only 9.0% including all stages, which is the lowest survival rate among all forms of cancer [1]. More importantly, pancreatic cancer is generally diagnosed at late stages, which greatly shortens the life-span of patients. Developing methods to detect and monitor pancreatic cancer is more critical for improving the survival rate than improving therapeutic regimens which are nevertheless unable to assist in advanced stages of the disease.

As general anatomical imaging strategies, ultrasonography, magnetic resonance imaging (MRI), near infrared imaging (NIR), and computed tomography (CT) have been widely employed for cancer diagnosis, especially the triphasic CT that has already been used for the initial detection of pancreatic cancer [2–5]. However, these imaging modalities have limits to their sensitivity and specificity to cancerous cells. Conversely, highly sensitive and non-invasive images are easily generated at the molecular level via positron emission tomography (PET) imaging [6–8]. The broad-spectrum PET tracer, ^{18}F-fluorodeoxyglucose, has been widely used in the clinic for tumor scanning [9–11]. Nevertheless, these results could be misleading due to physiological differences (e.g., glucose metabolism) among individuals [12]. Notably, the method of antibody-based PET (i.e., immunoPET) can selectively detect malignant tissue by targeting specific cancer surface makers, for instance,

human epidermal growth factor receptor 2 (HER2), which may offer an effective strategy for pancreatic cancer detection [13].

Trophoblast cell-surface antigen 2 (Trop-2) is a transmembrane glycoprotein that is overexpressed in various solid cancer cells such as pancreatic and breast carcinoma [14]. It is known that tumor progression, including behaviors such as cell proliferation and invasion, are promoted by high expression of Trop-2 [14–16]. Additionally, Trop-2 expression is already a prognostic factor for various carcinomas, including pancreatic cancer [17, 18]. Recently, the Trop-2 antibody–drug conjugate (ADC), sacituzumab govitecanhziy, successfully targeted this antigen and induced positive response in patients with metastatic triple-negative breast cancer [19]. Thus, Trop-2 plays a key role in cancer progression, which gives it significant potential as a target for cancer diagnosis, treatment monitoring, and therapy (e.g., ADC and radioimmunotherapy via ^{177}Lu or ^{90}Y conjugation). To date, the investigation of Trop-2-targeted immunoPET has been limited, with only a few studies investigating fragment antigen-binding (Fab) fragment of anti-Trop-2 antibodies as potential PET tracers for prostate cancer imaging [20, 21]. Notably, there are no reports about Trop-2 based immunoPET for pancreatic cancer detection.

We developed and evaluated an immunoPET strategy for pancreatic carcinoma detection via ^{89}Zr-DFO-AF650 (an antibody that binds to Trop-2) tracer, showing a highly efficient method of imaging cancerous lesions. Our findings demonstrate that immunoPET via ^{89}Zr-labeled Trop-2 antibody may allow physicians to detect Trop-2-positive pancreatic cancer at earlier stages as well as monitor the status of malignant lesions after therapy.

Materials and methods

Deferoxamine (DFO) conjugation and ^{89}Zr-labeling of AF650

The conjugation of DFO and ^{89}Zr labeling of AF650 were conducted via the same strategies reported previously [6]. In brief, anti-human Trop-2 antibody (Goat IgG) AF650 (Research and Diagnostic Systems, Inc.) was mixed with p-SCN-Bn-DFO in dimethyl sulfoxide (DMSO) at a molar ratio of 1:15 (pH 8.5 ~ 9.0), followed by 2-h incubation at room temperature. The resulting product was purified via PD-10 desalting cartridge. ^{89}Zr was generated by a PET trace cyclotron (GE Healthcare, Milwaukee, WI) via the ^{89}Y(p,n)^{89}Zr reaction. To radiolabel DFO-AF650, around ~ 37 MBq (~ 1 mCi) of ^{89}Zr was added to 0.5 mM HEPES buffer (pH 7.0) and incubated with DFO-AF650 (~ 150 ug) at 37 °C for 60 min. ^{89}Zr-DFO-AF650 was purified via a PD-10 column. As a nonspecific antibody, Goat serum IgG was employed and radiolabeled via the same strategy, which will be referred to as ^{89}Zr-DFO-IgG.

Cell culture

Human pancreatic cancer cell lines including BxPC-3, AsPC-1, and MIA PaCa-2 cells were obtained from the American Type Culture Collection (ATCC) (Manassas, VA, USA). Cells were cultured in standard RPMI-1640 or Dulbecco’s modified Eagle’s medium (DMEM) with 10% fetal bovine serum (FBS) (GE Healthcare, Chicago, IL, USA) as a supplement at 37 degrees with 5% CO_2.

Western blot

BxPC-3, AsPC-1, and MIA PaCa-2 cells were harvested and suspended in lysis buffer (BioRad). Total protein concentrations were detected via the BCA protein assay kit (Thermo Fisher Scientific). Certain amounts of each protein were separated by Bis–Tris plus gel (Thermo Fisher Scientific) via electrophoresis and then detected via first (AF650 and Beta-actin, Novus Biologicals) and secondary (Donkey antiGoat/mouse IgG-DyLight 800/680, Novus Biologicals) antibodies. The resulting membrane was detected and scanned on a LI-COR Odyssey infrared imaging system (LI-COR Biosciences).

Flow cytometry

BxPC-3, AsPC-1, and MIA PaCa-2 cells were washed and re-suspended in eBioscience™ flow cytometry staining buffer (Thermo Fisher) at a final concentration of 10^5 cells/mL. Immunostaining of cells was conducted by using AF650, AF650-DFO, and donkey anti-Goat IgG-Alexa Fluor 488 at final concentrations of 10 and 5 μg/mL. Cells after staining were examined on a MACSQuant cytometer (Miltenyi Biotec). The data and plots were analyzed by the FlowJo software.

AF650 saturation binding assay

Briefly, BxPC-3 cells were added into a 96-well filter plate (Corning®) with a concentration of 100,000 cells per well. Then, a series of ^{89}Zr-DFO-AF650 solutions (PBS with 0.1% BSA) were prepared, and cells were incubated in these solutions for 2 h at room temperature, with different final concentrations ranging from 0.03 to 100 nM. In parallel, unlabeled AF650 (1 μM) was added for determination of nonspecific binding. After incubation, cells were washed and analyzed via the gamma counter (PerkinElmer). According to the overall and nonspecific bindings, the surface expression of Trop-2, K_d, and B_{max} were identified in GraphPad Prism (version 8.0) software.

Animal models

All procedures associated with animals were conducted with protocols approved by the University of Wisconsin Institutional Animal Care and Use Committee. Female athymic nude mice (4 ~ 6 weeks) were used in this study. Briefly, the BxPC-3, AsPC-1, and MIA PaCa-2 cells were harvested and engrafted (2×10^6 cells) into the lower right flank subcutaneously with Matrigel (BD Biosciences). For the orthotopic BxPC-3 xenograft model, an incision was made on the left side of the mice under anesthesia. Then, 1 million cells mixed with Matrigel were slowly administered into the pancreas. On a weekly basis, the development of orthotopic tumors was monitored using ultrasound (Vevo 2100).

PET/CT, biodistribution, and imaging analysis

The mice bearing tumor (subcutaneous (S.C.) and orthotopic model) was intravenously administered with 5.5 ~ 7.4 MBq of ^{89}Zr-DFO-AF650 or ^{89}Zr-DFO-IgG and scanned on an Inveon micro-PET/CT rodent model scanner (Siemens Medical Solutions) at several intervals (4, 24, 48, 72, 96, and 120 h) post injection. After 5-day scanning, the major organs (e.g., the heart, spleen, kidney, liver, and tumor) were harvested for quantification of the tracer accumulated on PET/CT scanner or a gamma counter (PerkinElmer). The

biodistribution (BioD) among organs was analyzed and presented as a percentage of injected dosage/gram of organ (%ID/g). Size of tumor was calculated by following formula: 1/2(length × width^2). The region of interest (ROI) were drawn on key tissues (including the heart, spleen, kidney, liver, tumor, and muscle) for studying the pharmacokinetics of ^{89}Zr-DFO-AF650. The linear regression (ROI and BioD) and heat map (ROI) analysis were also performed for further confirmations of the correlation (ROI and BioD) and ROI significance among Trop-2-positive and Trop-2-negative groups.

Immunofluorescence staining

Tumors of BxPC-3, AsPC-1, and MIA PaCa-2 were collected and embedded in the optimal cutting temperature compound (OCT compound). Frozen Sects. (5 mm) of tumor tissues were processed by the Experimental Pathology Laboratory, Carbone Cancer Center, University of Wisconsin. Obtained specimens were treated via the general immunofluorescence staining procedure. Briefly, the slides were fixed and washed with 4% paraformaldehyde (PFA) and PBS, respectively. After blockage with 10% donkey serum, samples were incubated with AF650 and CD31 antibody with final concentration at 10 μg/mL (Thermo Fisher Scientific) at 4 degrees overnight. The specific secondary antibodies with Alexa Fluor 488 or Cy3 were applied for developing immunofluorescence. Finally, the immunofluorescence images of sections were obtained on a Nikon A1R confocal microscope (Nikon).

Statistical analysis

All the data were analyzed on PRISM 8 (GraphPad) via unpaired student *t* test, one- or two-way ANOVA analysis. *P* values < 0.05 were considered as statistically significant.

Results

Trop-2 expression and binding affinity of AF650 in pancreatic cancer cells

To identify the relative expression of Trop-2 among various pancreatic cancer cells, AF650 was employed as the primary antibody for detection. As shown in Fig. 1a, Trop-2 was highly expressed in BxPC-3 cancer cells, while its expression was hardly detected in AsPC-1 and MIA PaCa-2. More specifically, the expression level in BxPC-3 cells was more than 4 and 20 times higher than those in AsPC-1 and MIA PaCa-2 cells, respectively (Figure S1). It was found that AF650 could selectively bind to BxPC-3 cells, which is indicated by a significant shift in the fluorescent signal peak, suggesting that AF650 is highly efficient in detecting Trop-2-positive cells (Fig. 1b). It is notable that DFO conjugation did not affect the binding efficiency of AF650. In comparison, the AF650-based signal slightly shifted in AsPC-1 and MIA PaCa-2 cells.

To further evaluate the binding affinity of AF650, a saturation binding assay was conducted in BxPC-3 cells with highly-expressed Trop-2. Figure 1c shows that the ^{89}Zr-DFO-AF650 could attach to BxPC-3 cells effectively, with a Trop-2 affinity constant (K_d) at 22.34 ± 2.51 nM. The amount of expressed Trop-2 was also determined as (0.70 ± 0.03) × 10^6 receptors/cell.

ImmunoPET imaging and biodistribution of ^{89}Zr-DFO-AF650 in mice bearing subcutaneous tumors

To further evaluate its targeting efficiency, ^{89}Zr-DFO-AF650 was employed for imaging various pancreatic cancers in a subcutaneous xenograft mice model. Before the final scanning, a series of PET scans had been completed at 4, 24, 48, 72, 96, and 120 h post injection of the tracer. Meanwhile, the biodistribution of tracer among various organs was defined at the last time point. As shown in Fig. 2a, the circulation of ^{89}Zr-DFO-AF650 was desirable, with clear signals at the blood pool. It is noteworthy that it accumulated in BxPC-3 tumors just after 4 h (11.7 ± 1.23%ID/g) and eventually reached 19.3 ± 2.21%ID/g at 120 h post injection (Fig. 2a–b) ($n = 4$), which was significantly higher than those in the other two tumors ($P < 0.0001$ at all time points). In comparison, ^{89}Zr-DFO-AF650 rarely attached to AsPC-1 and MIA PaCa-2 tumors due to the low expression level of Trop-2, with the highest accumulation at 3.12 ± 0.71 and 4.70 ± 1.14%ID/g, respectively (Fig. 2a–b) ($n \geq 3$).

Similarly, the biodistribution (BioD) assays at day 5 further confirmed that ^{89}Zr-DFO-AF650 was particularly selective to BxPC-3 tumors rather than the others, showing 28.8 ± 7.63, 3.51 ± 0.69, and 6.76 ± 2.08%ID/g in BxPC-3, AsPC-1, and MIA PaCa-2 tumors, respectively ($P < 0.0001$) (Fig. 2c) ($n \geq 3$). Nevertheless, both PET and BioD tracer kinetics were similar among the three different tumors in various organs (Fig. 2).

As a negative control, the nonspecific antibody, ^{89}ZrDFO-IgG was recruited (Figure S2). Obviously, the uptake of ^{89}Zr-DFO-IgG in BxPC-3 tumor was much lower than that of ^{89}Zr-DFO-AF650, with PET and BioD values at 6.90 ± 1.28 and 8.66 ± 4.95%ID/g, respectively (Figure S2) ($n = 3$). This affirms that ^{89}Zr-DFO-AF650 is highly selective to BxPC-3 malignant tissues.

Immunostaining of Trop-2 and CD31 in tumor tissues

For confirmation of the Trop-2 expression and growth status of cancerous tissues, three tumor sections were stained with Trop-2 and CD31 antibodies. As can be seen in Fig. 3, the Trop-2 was greatly expressed in the BxPC-3 malignant lesion, but not on AsPC-1 and MIA PaCa-2 cancer cells. This is well correlated to the trend of trace uptake by three tumors. Meanwhile, extensive blood vessels (CD31) were observed among three cancer models, showing the active growth stage of tumors.

ImmunoPET and biodistribution assays of ^{89}Zr-DFO-AF650 in the orthotopic tumor mice model

Considering the different environments between pancreatic and subcutaneous tissues, the orthotopic BxPC-3 tumor model was established for evaluating the Trop-2 targeting efficiency of ^{89}Zr-DFO-AF650 in a real pancreatic cancer case. According to the PEC/CT, accumulation of tracer in BxPC-3 tumors gradually increased from 8.35 ± 1.61 to 18.1 ± 4.00%ID/g during the period of 120 h after injection (Fig. 4). Notably, the ^{89}Zr-DFO-AF650 was able to detect the tumor with a size around 45 mm^3 via immunoPET, showing a clear signal (17.5%ID/g) within the tumor on day 5 (Figure S3). Meanwhile, the kinetics of tracer among organs were similar to previous data (Fig. 4b).

The ex vivo PET scanning further identifies the accumulation of ^{89}Zr-DFO-AF650 within orthotopic pancreatic cancer lesions, while signals were hardly detected in surrounding organs including the pancreas and spleen (Fig. 5a–b). Similarly, the BioD data indicates that the tracer accumulated in tumors reached 26.0 ± 6.43%ID/g at 120 h post injection (Fig. 5c). In comparison, ^{89}Zr-DFO-AF650 rarely attached to the normal pancreatic tissue with a BioD signal at only 3.20 ± 1.40%ID/g, which is similar to other organs. This suggests that the present method is capable of efficiently detecting and distinguishing pancreatic malignant lesions from normal pancreatic cells.

Evaluation of Trop-2 immunoPET for detecting pancreatic cancer via ^{89}Zr-DFO-AF650

To systemically evaluate the potential of Trop-2 targeting immunoPET in pancreatic cancer diagnosis, the correlation of PET and BioD assays of ^{89}Zr-DFO-AF650 was further examined. As shown in Fig. 6a, a good concordance could be observed in terms of tumor signal, showing an R square at 0.9444 ($P < 0.0001$). For defining the sensitivity and efficiency in tumor detection, a series of heat maps and receiver operating characteristic (ROC) curves had been generated from PET ROI data as well (Fig. 6b and Figure S4–5). The heat map profiles could efficiently classify and distinguish the BxPC-3 bearing mice (including both subcutaneous and orthotopic models) with ^{89}Zr-DFO-AF650 from other groups at only 4 h post injection. This finding indicates the high efficiency of Trop-2 targeting immunoPET, which is consistent with the outcome from receiver operating characteristic (ROC) curves (with 100% sensitivity and specificity, > 6.50%ID/g) (Figure S5). These clearly illustrate the accuracy of performed Trop-2 immunoPET for detecting pancreatic cancers and its promising feasibility in future clinic applications.

Discussion

In the current study, ^{89}Zr-DFO-AF650 was recruited and systemically studied as an immunoPET tracer for imaging Trop-2-positive pancreatic cancer. Of the three pancreatic cancer cell lines, BxPC-3 expressed high levels of Trop-2, while AsPC-1 and MIA PaCa-2 seemed to have minimal expression of Trop-2. ^{89}Zr-DFO-AF650 was able to bind the BxPC-3 malignant cells with 28.8 ± 7.63%ID/g tracer accumulation, which was about 4.26 and 8.20 times higher than those of MIA PaCa-2 and AsPC-1, respectively. Moreover, ^{89}Zr-DFO-AF650 could effectively and specifically detect the malignant lesions in orthotopic xenograft tumor model, including a small tumor with a size of about 45 mm ^{3}. More importantly, results obtained from immunoPET greatly correlated to the ex vivo biodistribution results, which could efficiently identify Trop-2-positive tumors from others. These findings suggest that Trop-2 targeting immunoPET is viable for use in the diagnosis and monitoring of Trop-2-positive pancreatic cancer.

Trop-2 is vitally important for tumor progression, yet there are few studies of non-invasive cancer imaging with Trop-2 (fab fragment) in comparison to other tumor targets such as HER2 (human epidermal growth factor receptor 2) and VEGFR2 (vascular epithelial growth factor receptor 2) [20–24]. Nevertheless, these studies have all been conducted on subcutaneous prostate cancer models. Specifically, the Trop-2 Fab was able to target S.C. PC-3 tumor with a 20.0%ID/g tumor uptake at 16 h post injection [20]. Similarly, our

current study shows that the BxPC-3 (Trop-2 positive) tumor signal was 20.4 ± 1.22%ID/g at 1 day after injection (Fig. 2).

Considering the overexpression of Trop-2 in cancerous cells and patients with pancreatic cancer (≥ 55%, n = 197) [25], the development of Trop-2-based immunoPET for diagnosis of pancreatic carcinoma is very promising. Especially, the tumor tissues with higher grades exhibit more abundant expression of Trop-2. The percentage of positive staining increases obviously from 48 to 77% when pancreatic cancer develops from stage T2 to T4. All these suggest that quantitative imaging of Trop-2 in vivo can faithfully reflect the variable concentration of Trop-2 in pancreatic cancer tissues of different stages. It also implies that early detection of pancreatic cancer based on in vivo characterization of Trop-2 expression at relatively early stages is possible. Notably, its targeting efficiency (~ 20.0%ID/g) is higher than other reported immunoPET targets such as tissue factor and insulin-like growth factor 1 receptor (IGF-1R), which achieve signals of 16.5 ± 2.6 and 8.24 ± 0.51%, respectively [26, 27]. Moreover, Trop-2 expression levels are highly related to the prognosis of patients with pancreatic carcinoma [25], suggesting that, in addition detection of pancreatic cancer, this method may also be used to help monitor prognosis.

Furthermore, the monitoring period of this method is strongly associated with the isotope of selection. Compared to an isotope with a short half-life, such as ^{64}Cu (12 h), an isotope with a longer half-life, such as ^{89}Zr (about 3.3 days), would be more favorable for use in a clinical setting [6, 28]. It was shown in this study that the accumulation of tracer in BxPC-3 S.C. tumors quickly achieved the plateau phase just 24 h post injection, but it took more than 72 h for ^{89}Zr-DFO-AF650 to reach peak value in BxPC-3 orthotopic tumors (Figs. 2 and 4). As malignant lesions generated in the original organ could well mimic the real cancer, the findings obtained from the orthotopic model should be more reliable and accurate. Therefore, Trop-2 immunoPET may require more than 3 days to obtain the most accurate image in a clinical setting. In addition, long-term scanning is highly recommended for monitoring the prognosis of patients after treatment. For these reasons, ^{89}Zr-labeled tracer is particularly suitable for Trop-2 immunoPET imaging. It is notable that the efficiency of Trop-2-mediated immunoPET was investigated in the orthotopic model first, which would offer more information for future translation of Trop-2-based cancer imaging. In addition to the application of PET imaging, the highly specific accumulation would also enable the feasibility of Trop-2 based radioimmunotherapy by conjugating isotopes like ^{177}Lu, ^{90}Y, and ^{225}Ac.

An important observation in this study was that ^{89}ZrDFO-AF650 was able to detect a tiny tumor (≤ 45 mm^3) in the orthotopic tumor model (Figs. 4 and S3). Generally, patients with pancreatic cancer (stage 1A) have tumors that are smaller than 20 mm in diameter, with a life expectancy of 17.2 ± 8.2 months [29]. Once the tumor reaches a certain size (≥ 30 mm), the life expectancy dramatically decreases to 7.6 ± 1.2 months (P = 0.021). Thus, a sensitive detection method such as Trop-2-mediated immunoPET may improve detection of pancreatic cancerous lesions with small diameter and extend the life expectancy of patients. Furthermore, immunoPET via ^{89}Zr-DFO-AF650 was correlated to the real distribution of Trop-2 in cancerous tissues and showed a high selectivity in distinguishing Trop-2-positive cancerous tissues (Fig. 6). In the recent past, various tracers have been

successfully employed in immunoPET for tumor detection, but somehow many studies fail to systemically evaluate their sensitivity and accuracy as a diagnosis strategy [13]. In contrast, the performance of Trop-2 targeting immunoPET confirms its feasibility in the clinic for pancreatic cancer diagnosis.

In the last three decades, the average size of pancreatic tumors after diagnosis was 31 mm [30]. With the help of multidetector computed tomography (MDCT), pancreatic lesions that are smaller than 20 mm can be detected [31]. However, such precision detection of pancreatic cancer cannot be achieved with general anatomical imaging approaches. Although the current tracer, ^{89}Zr-DFO-AF650, cannot be further translated for clinical usage due to its immunogenicity issues, our findings systemically evaluated and confirmed the feasibility of the Trop-2 targeting immunoPET via a ^{89}Zr-radiolabelling strategy. Therefore, this study may accelerate and promote the real translation of Trop-2-mediated immunoPET in the clinic and eventually improve small lesion detection and monitoring of pancreatic cancer.

It is known that the expression of Trop-2 in normal tissues is significantly lower than that in the cancerous tissue. However, the xenograft models employed in this study are established using mouse species, and our tracer was derived from an anti-human Trop-2 antibody. Therefore, a potential limitation of the current experimental design is the lack of consideration of possible existence of antigen sink in patients, which should be investigated in detail in future preclinical/clinical studies.

Conclusion

In the current study, we investigated the efficiency of ^{89}Zr-DFO-AF650 as an immunoPET tracer for monitoring in vivo Trop-2 expression in pancreatic cancer. ^{89}Zr-DFO-AF650 specifically, rapidly, and persistently accumulated in Trop-2-positive tumors (BxPC-3) either in subcutaneous or orthotopic xenograft models. Notably, data well correlated between the immunoPET and the real bio-distribution of tracer, demonstrating the high sensitivity and accuracy of Trop-2 based immunoPET in detecting malignant pancreatic tissues, as well as small lesions. These findings suggest that the immunoPET via Trop-2 targeting could be employed for the sensitive detection and monitoring of pancreatic malignancies.

Supplementary Material

Refer to Web version on PubMed Central for supplementary material.

Acknowledgments

Funding This study is financially supported by the University of Wisconsin-Madison and the National Institutes of Health (P30CA014520).

References

1. Siegel RL, Miller KD, Jemal A. Cancer statistics, 2020. CA Cancer J Clin. 2020;70:7–30. [PubMed: 31912902]

2. Vincent A, Herman J, Schulick R, Hruban RH, Goggins M. Pancreatic cancer. Lancet. 2011;378:607–20. [PubMed: 21620466]
3. Chen W, Ni D, Rosenkrans ZT, Cao T, Cai W. Smart H2S-triggered/therapeutic system (SHTS)-based nanomedicine. Adv Sci. 2019;6:1901724.
4. Sun T, Jiang D, Rosenkrans ZT, Ehlerding EB, Ni D, Qi C, et al. A melanin-based natural antioxidant defense nanosystem for theranostic application in acute kidney injury. Adv Funct Mater. 2019;29:1904833.
5. Wang YXJ, Huang H, Zheng CJ, Xiao BH, Chevallier O, Wang W. Diffusion-weighted MRI of the liver: challenges and some solutions for the quantification of apparent diffusion coefficient and intravoxel incoherent motion. Am J Nucl Med Mol Imaging. 2021;11:107–42. [PubMed: 34079640]
6. Li M, Jiang D, Barnhart TE, Cao T, Engle JW, Chen W, et al. Immuno-PET imaging of VEGFR-2 expression in prostate cancer with (89)Zr-labeled ramucirumab. Am J Cancer Res. 2019;9:2037–46. [PubMed: 31598404]
7. Ni D, Wei H, Chen W, Bao Q, Rosenkrans ZT, Barnhart TE, et al. Ceria nanoparticles meet hepatic ischemia-reperfusion injury: the perfect imperfection. Adv Mater. 2019;31:1902956.
8. Jiang D, Im H-J, Boleyn ME, England CG, Ni D, Kang L, et al. Efficient renal clearance of DNA tetrahedron nanoparticles enables quantitative evaluation of kidney function. Nano Res. 2019;12:637–42. [PubMed: 32055285]
9. Gelezhe PB, Blokhin IA, Marapov DI, Morozov SP. Quantitative parameters of MRI and (18)F-FDG PET/CT in the prediction of breast cancer prognosis and molecular type: an original study. Am J Nucl Med Mol Imaging. 2020;10:279–92. [PubMed: 33329930]
10. Paul DM, Ghiuzeli CM, Rini J, Palestro CJ, Fung EK, Ghali M, et al. A pilot study treatment of malignant tumors using low-dose ^{18}F-fluorodeoxyglucose (18F-FDG). Am J Nucl Med Mol Imaging. 2020;10:334. [PubMed: 33329935]
11. Kaghazchi F, Borja AJ, Hancin EC, Bhattaru A, Detchou DKE, Seraj SM, et al. Venous thromboembolism detected by FDG-PET/CT in cancer patients: a common, yet life-threatening observation. Am J Nucl Med Mol Imaging. 2021;11:99–106. [PubMed: 34079639]
12. Belhocine T, Spaepen K, Dusart M, Castaigne C, Muylle K, Bourgeois P, et al. 18FDG PET in oncology: the best and the worst (Review). Int J Oncol. 2006;28:1249–61. [PubMed: 16596242]
13. Jiang D, Im H-J, Sun H, Valdovinos HF, England CG, Ehlerding EB, et al. Radiolabeled pertuzumab for imaging of human epidermal growth factor receptor 2 expression in ovarian cancer. Eur J Nucl Med Mol Imaging. 2017;44:1296–305. [PubMed: 28265738]
14. Goldenberg DM, Stein R, Sharkey RM. The emergence of trophoblast cell-surface antigen 2 (TROP-2) as a novel cancer target. Oncotarget. 2018;9:28989. [PubMed: 29989029]
15. Rapani E, Sacchetti A, Corda D, Alberti S. Human Trop-2 is a tumor-associated calcium signal transducer. Int J Cancer. 1998;76:671–6. [PubMed: 9610724]
16. Trerotola M, Cantanelli P, Guerra E, Tripaldi R, Aloisi A, Bonasera V, et al. Upregulation of Trop-2 quantitatively stimulates human cancer growth. Oncogene. 2013;32:222–33. [PubMed: 22349828]
17. Bignotti E, Todeschini P, Calza S, Falchetti M, Ravanini M, Tassi RA, et al. Trop-2 overexpression as an independent marker for poor overall survival in ovarian carcinoma patients. Eur J Cancer. 2010;46:944–53. [PubMed: 20060709]
18. Fong D, Moser P, Krammel C, Gostner JM, Margreiter R, Mitterer M, et al. High expression of TROP2 correlates with poor prognosis in pancreatic cancer. Br J Cancer. 2008;99:1290–5. [PubMed: 18813308]
19. Bardia A, Mayer IA, Vahdat LT, Tolaney SM, Isakoff SJ, Diamond JR, et al. Sacituzumab govitecan-hziy in refractory metastatic triple-negative breast cancer. N Engl J Med. 2019;380:741–51. [PubMed: 30786188]
20. van Rij CM, Lütje S, Frielink C, Sharkey RM, Goldenberg DM, Franssen GM, et al. Pretargeted immuno-PET and radioimmunotherapy of prostate cancer with an anti-TROP-2 x anti-HSG bispecific antibody. Eur J Nucl Med Mol Imaging. 2013;40:1377–83. [PubMed: 23674207]
21. Lütje S, Rijpkema M, Goldenberg DM, van Rij CM, Sharkey RM, McBride WJ, et al. Pretargeted dual-modality immuno-SPECT and near-infrared fluorescence imaging for image-guided surgery of prostate cancer. Cancer Res. 2014;74:6216–23. [PubMed: 25252911]

22. Zaman S, Jadid H, Denson AC, Gray JE. Targeting Trop-2 in solid tumors: future prospects. OncoTargets Ther. 2019;12:1781.

23. van Rij CM, Frielink C, Goldenberg DM, Sharkey RM, Franssen GM, Lütje S, et al. Pretargeted immunoPET of prostate cancer with an anti-TROP-2 x anti-HSG bispecific antibody in mice with PC3 xenografts. Mol Imaging Biol. 2015;17:94–101. [PubMed: 25060065]

24. van Rij CM, Frielink C, Goldenberg DM, Sharkey RM, Lütje S, McBride WJ, et al. Pretargeted radioimmunotherapy of prostate cancer with an anti-TROP-2× Anti-HSG bispecific antibody and a 177Lu-Labeled Peptide. Cancer Biother. 2014;29:323–9.

25. Fong D, Moser P, Krammel C, Gostner J, Margreiter R, Mitterer M, et al. High expression of TROP2 correlates with poor prognosis in pancreatic cancer. Br J Cancer. 2008;99:1290. [PubMed: 18813308]

26. Hong H, Zhang Y, Nayak TR, Engle JW, Wong HC, Liu B, et al. Immuno-PET of tissue factor in pancreatic cancer. J Nucl Med. 2012;53:1748–54. [PubMed: 22988057]

27. England CG, Kamkaew A, Im H-J, Valdovinos HF, Sun H, Hernandez R, et al. ImmunoPET imaging of insulin-like growth factor 1 receptor in a subcutaneous mouse model of pancreatic cancer. Mol Pharm. 2016;13:1958–66. [PubMed: 27054683]

28. Rosenkrans ZT, Cai W. Total-body PET imaging for up to 30 days after injection of ^{89}Zr-labeled antibodies. J Nucl Med. 2020;61:451–2. [PubMed: 31806778]

29. Agarwal B, Correa AM, Ho L. Survival in pancreatic carcinoma based on tumor size. Pancreas. 2008;36:e15–20.

30. Tummala P, Junaidi O, Agarwal B. Imaging of pancreatic cancer: an overview. J Gastrointest. 2011;2:168.

31. Chaudhary V, Bano S. Imaging of the pancreas: recent advances. Indian J Endocrinol Metab. 2011;15:S25. [PubMed: 21847450]

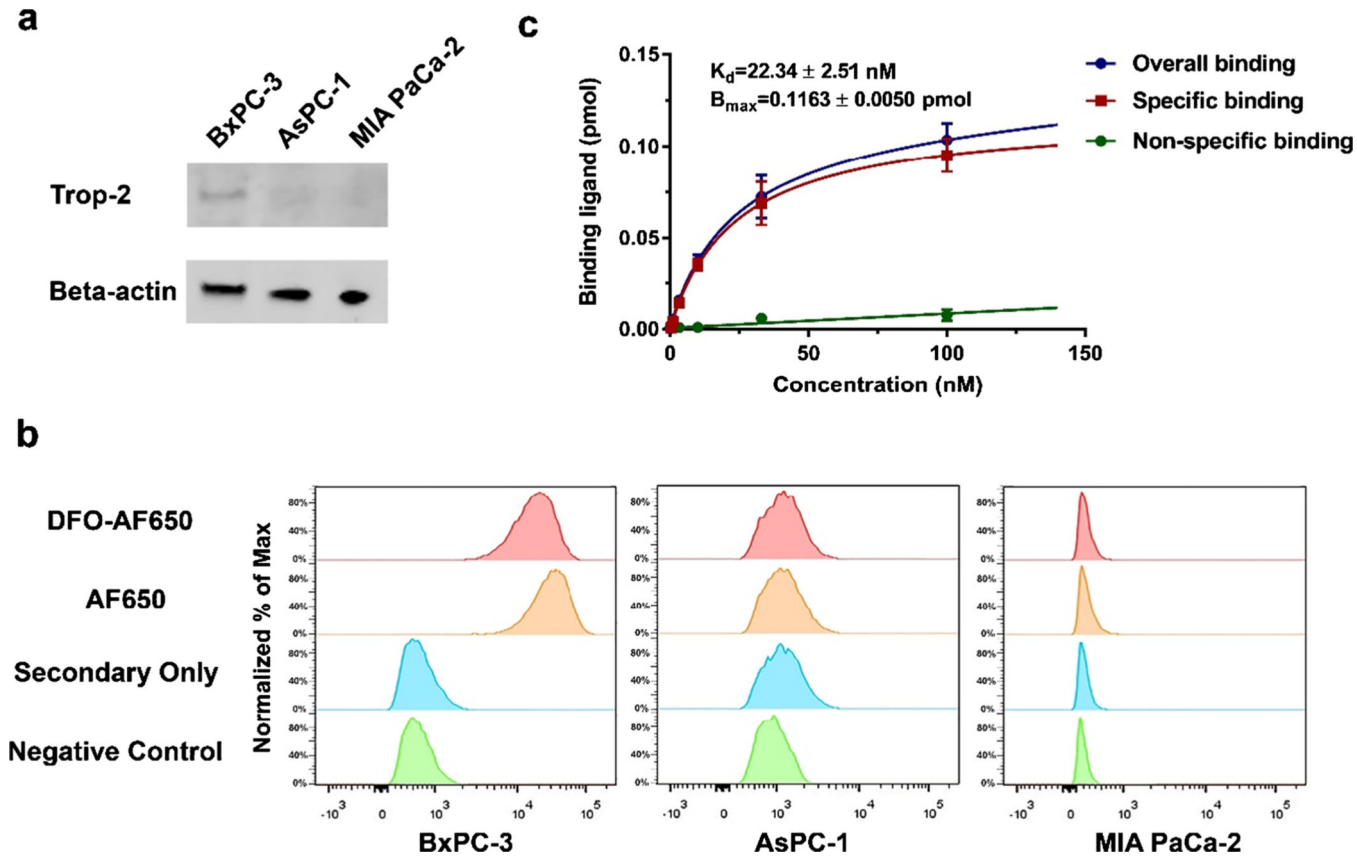

Fig. 1.

The binding affinity of AF650 to Trop-2. **a** The expression level of Trop-2 among three pancreatic cancer cell lines. **b** The Trop-2 expression among three cancer cell lines via DFO-AF650 or AF650 mediated flow cytometry. **c** The Trop-2 saturation binding assays of ^{89}Zr-DFO-AF650 on BxPC-3 cells; unlabeled DFO-AF650 was recruited for determining the nonspecific binding (n = 3)

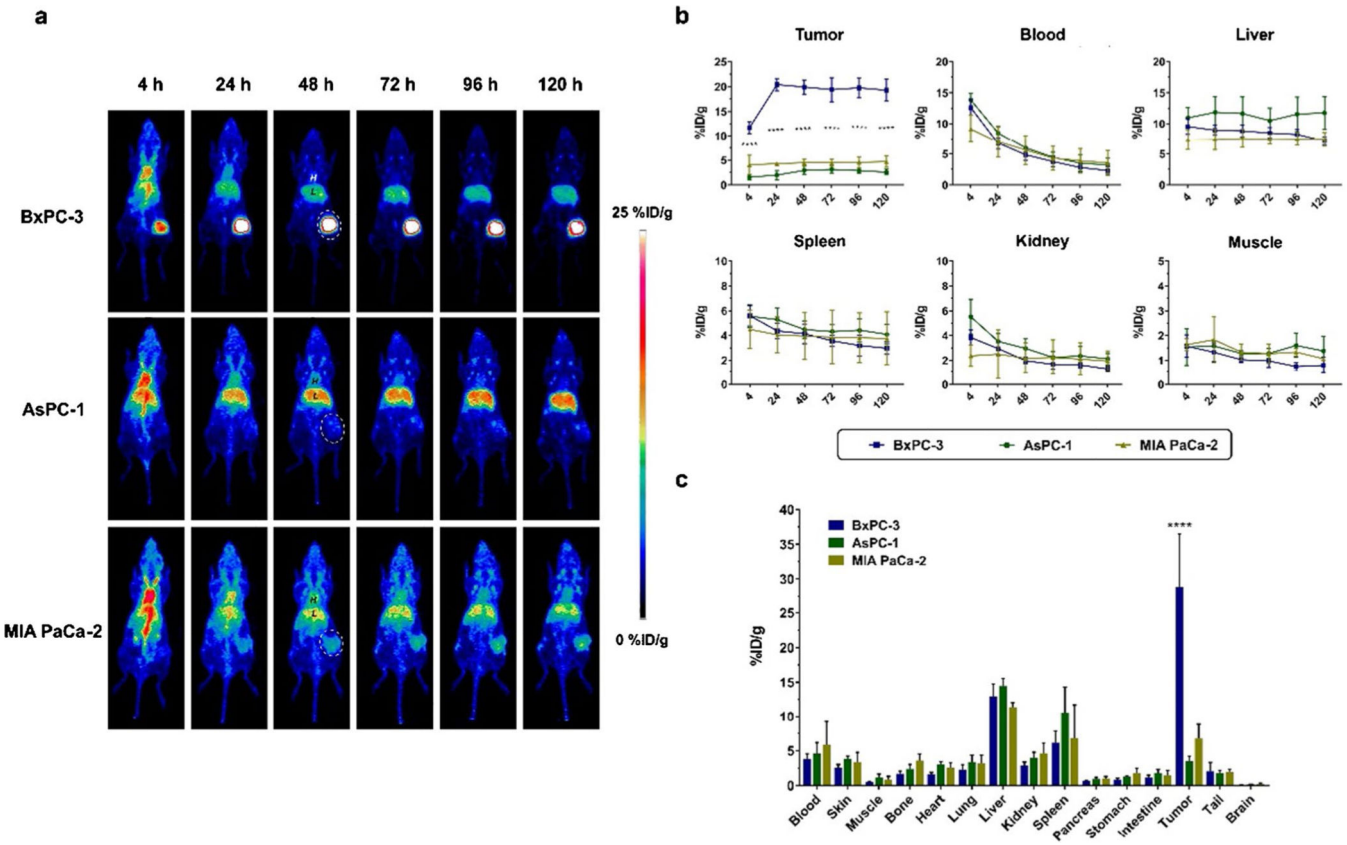

Fig. 2.

ImmunoPET of ^{89}Zr-DFO-AF650 among subcutaneous pancreatic cancer models. **a** The serial PET maximum intensity projection (MIP) images of ^{89}Zr-DFO-AF650 at 4, 24, 48, 72, 96, and 120 h post injection ($n \geq 3$); tumors are indicated by white dash circles, H, blood pool; L, liver. **b** The curves of PET region of interest (ROI) including the tumor, heart, liver, spleen, kidney, and muscle at different time points. **c** The bio-distribution of ^{89}Zr-DFO-AF650 among different organs harvested at day 5 ($n \geq 3$). **** shows $P < 0.0001$

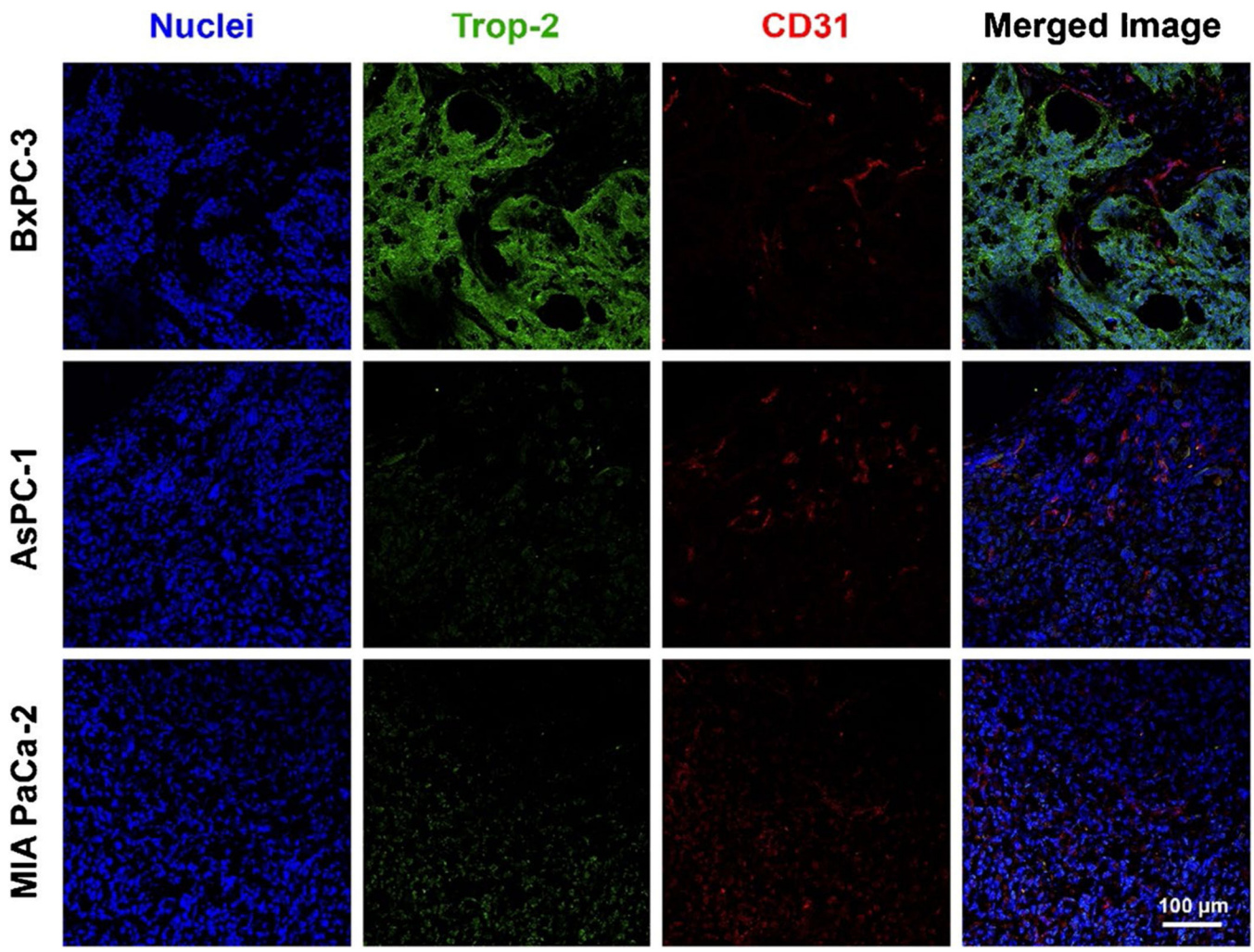

Fig. 3.

Trop-2 expression within tumor tissues from pancreatic cancer cells. The immunofluorescence staining of BxPC-3, AsPC-1, and MIA PaCa-2 tumor sections with DAPI (blue), Trop-2 (green), and CD31 (red) antibodies. Scale bar = 100 μm

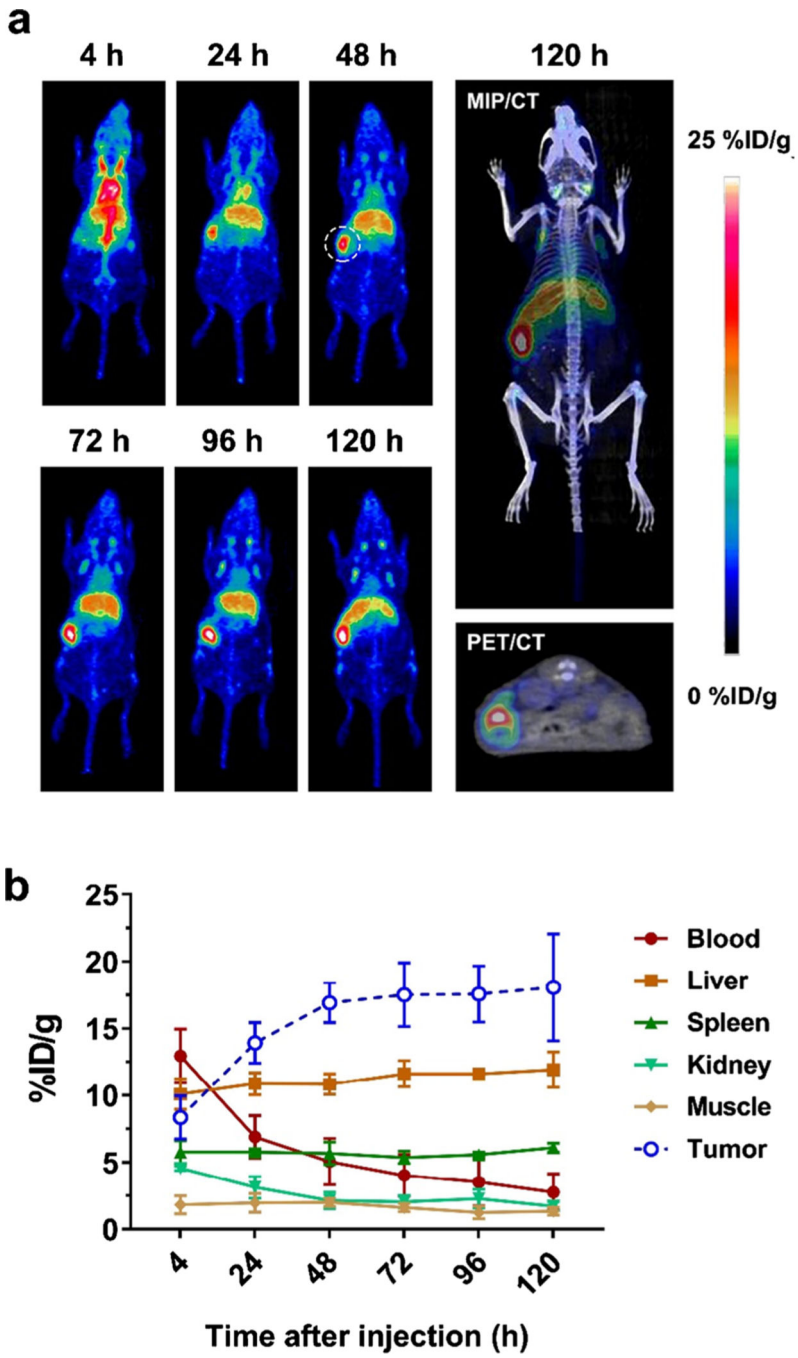

Fig. 4.

Evaluation of ^{89}Zr-DFO-AF650 in detecting BxPC-3 cancer cells in an orthotopic tumor model via ImmunoPET. **a** The MIP PET images of ^{89}Zr-DFO-AF650 in mice bearing BxPC-3 orthotopic tumors at different time points, and the representative MIP/CT and PET/CT images at day 5 (n = 4); the tumor site is highlighted by the dashed line. **b** The time-activity curves of PET ROI among organs from 4 to 120 h after initial tracer administration (n = 4)

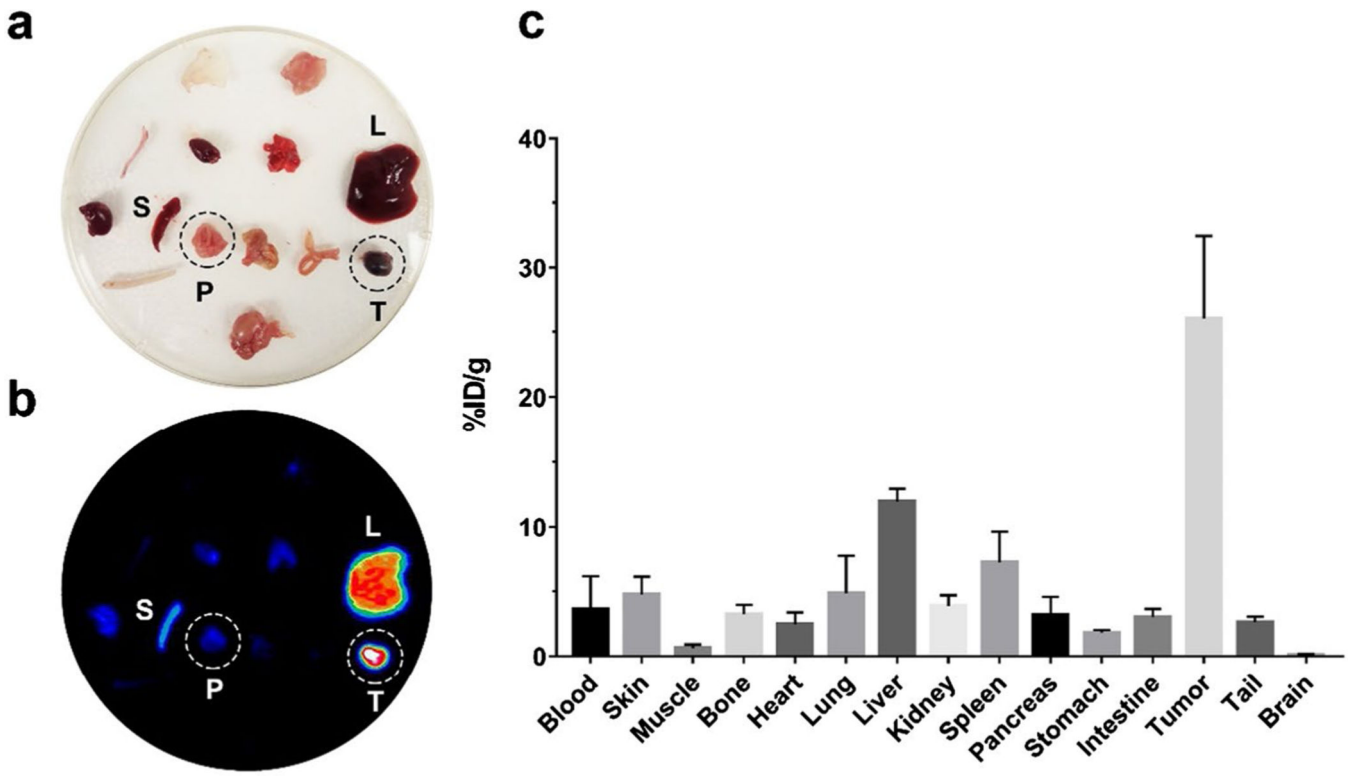

Fig. 5.

The high specificity of ^{89}Zr-DFO-AF650 in detecting the orthotopic BxPC-3 tumor. The (**a**) optical and (**b**) MIP PET images of tissues harvested from mice injected with ^{89}Zr-DFO-AF650 at day 5 ($n = 4$); **c** the bio-distribution of ^{89}Zr-DFO-AF650 tracer among organs collected at day 5 (= 4)

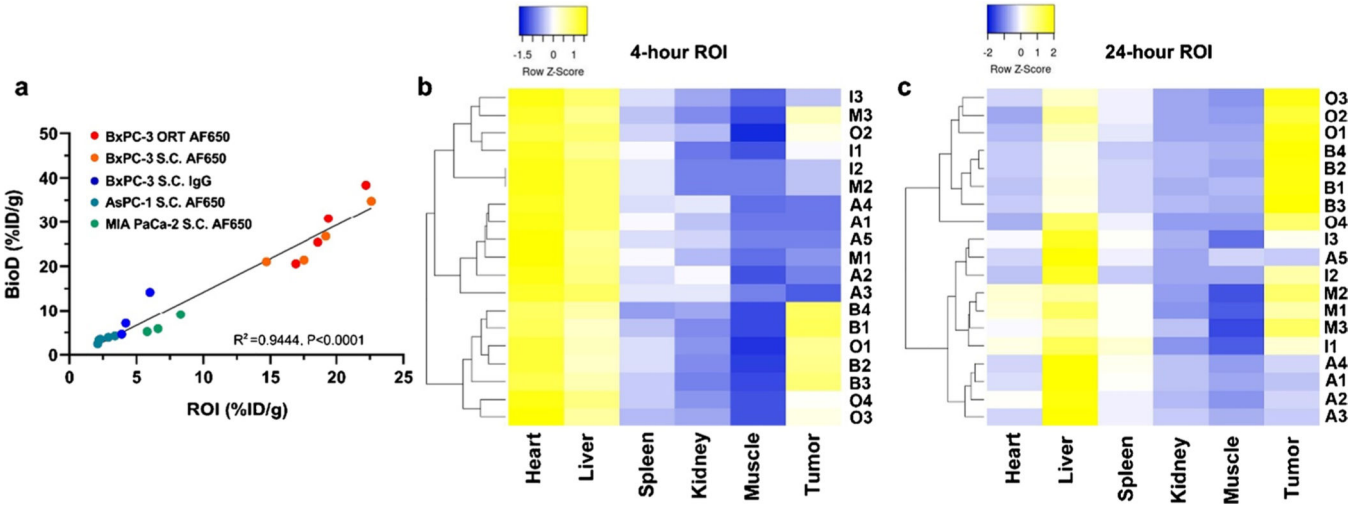

Fig. 6.

Evaluation of ^{89}Zr-DFO-AF650 imaging metrics for Trop-2 immunoPET among pancreatic cancer models. **a** The correlation between ROI and BioD (%ID/g); ORT, orthotopic model; S.C., subcutaneous model. **b–c** The Z-normalized heat map of ^{89}Zr-DFO-AF650 accumulated values in various organs via specified ROI (%ID/g) at 4 and 24 h post injection; groups including A: AF650 (AsPC-1, S.C.), B: AF650 (BxPC-3, S.C.), I: IgG (BxPC-3, S.C.), M: AF650 (MIA PaCa-2, S.C.), O: AF650 (BxPC-3, ORT)